Remote Sensing of the Surface Wind Field over the Coastal Ocean via Direct Calibration of HF Radar Backscatter Power

ANTHONY KIRINCICH

Woods Hole Oceanographic Institution, Woods Hole, Massachusetts

(Manuscript received 20 November 2015, in final form 23 March 2016)

ABSTRACT

The calibration and validation of a novel approach to remotely sense surface winds using land-based high-frequency (HF) radar systems are described. Potentially available on time scales of tens of minutes and spatial scales of 2–3 km for wide swaths of the coastal ocean, HF radar–based surface wind observations would greatly aid coastal ocean planners, researchers, and operational stakeholders by providing detailed real-time estimates and climatologies of coastal winds, as well as enabling higher-quality short-term forecasts of the spatially dependent wind field. Such observations are particularly critical for the developing offshore wind energy community. An autonomous surface vehicle was deployed within the Massachusetts Wind Energy Area, located south of Martha's Vineyard, Massachusetts, for one month, collecting wind observations that were used to test models of wind-wave spreading and HF radar energy loss, thereby empirically relating radar-measured power to surface winds. HF radar–based extractions of the remote wind speed had accuracies of 1.4 m s^{-1} for winds less than 7 m s^{-1}, within the optimal range of the radar frequency used. Accuracies degraded at higher winds due to low signal-to-noise ratios in the returned power and poor resolution of the model. Pairing radar systems with a range of transmit frequencies with adjustments of the extraction model for additional power and environmental factors would resolve many of the errors observed.

1. Introduction

Land-based high-frequency (HF) coastal ocean radar systems have proven to be highly effective at measuring ocean surface currents on an operational basis. At present, over 130 systems operate within the coastal waters of the United States, providing detailed maps of real-time currents at resolutions of 2–8 km and offshore distances up to 150 km. However, these instruments also have the potential to provide estimates of the spatially variable surface wind field (Barrick 1972), likely at ranges up to 100 km offshore. This work seeks to exploit variations in the power of the radar's return due to short ocean waves to estimate winds via direct calibration. The use of empirical approaches such as this are now possible due to new technology enabling mobile in situ wind observations that drastically lower the cost of obtaining the calibration data required to validate models relating the power of the HF radar return to the wind speed. Thus, this work would enable a feature of radar returns that has been known for more than 50 years to be exploited for operational use.

While the surface wind field over the coastal ocean has potentially large spatial scales over time scales of tens of hours, on time scales of tens of minutes, spatial scales can be much shorter due to the passage of fronts and/or low-level jets (e.g., Edson et al. 2007). Knowledge of winds on these time and space scales is of particular interest to newer coastal ocean stakeholders, such as the developers and operators of offshore wind energy facilities. Wind energy developers require potentially dense "hub height" observations in order to obtain the financial backing necessary for projects to move forward. This requirement presents a difficult hurdle for offshore wind energy projects to overcome, as the costs associated with in situ observations at hub height (i.e., erecting multiple towers or fixed platforms in the coastal ocean) solely for resource characterization can be prohibitively high. Recent work (see Beaucage et al. 2012) has shown that atmospheric models can produce a state estimate of the atmospheric boundary layer capable of accurately modeling hub-height wind power levels. Yet, the ability of this type of state estimate to accurately

Corresponding author address: Anthony Kirincich, Department of Physical Oceanography, Woods Hole Oceanographic Institution, 266 Woods Hole Rd., Woods Hole, MA 02543-1050.
E-mail: akirincich@whoi.edu

DOI: 10.1175/JTECH-D-15-0242.1

forecast or hindcast the wind field is a function of the amount and quality of wind and temperature data being used to guide the model solution. Second, both wind farm and grid operators require short-term forecasts of the power output of an operating wind farm to balance loading of the electrical grid and minimize uncertainty. The potential spatially and temporally dense estimates of surface winds that a calibrated HF radar system could provide to a data-assimilating nested atmospheric model might be sufficient to constrain the hub-height predictions to the accuracies required for both near-term forecasts and resource characterization. Additionally, the direct observations of surface winds themselves would be operationally useful for informing construction and maintenance activities.

The dependence of HF radar backscatter power on wind speed and direction has been known for some time (Barrick 1972; Barrick and Weber 1977; Heron and Rose 1986; Harlan and Georges 1994; Wyatt 2012; among others). A changing wind direction alters the relative power returned from waves directed toward and away from the radar, thus knowledge of this difference and a wind-wave spreading model has been used to predict wind direction (Heron and Rose 1986; Harlan and Georges 1994; Paduan et al. 1999). In contrast, the dependence of power on wind speed has traditionally been thought to be both spatially and temporally variable, as well as dependent on unknown radar-specific parameters. However, Shen et al. (2012) and Kirincich (2013) recently illustrated that in situ wind data can be used to calibrate the backscatter power of individual radar sensors, enabling estimates of wind speed via empirical calibration. While these efforts documented the short spatial scale of the calibration's validity, they also demonstrated that, to the accuracy of the radar observations themselves, only small amounts of in situ observations were needed to produce a sufficient calibration. Thus calibrations via newly available mobile platforms represent a potentially cost-effective way to empirically link the locally relevant changes in radar power with wind speed over the broad spatial area observed by a radar system.

The goal of this study was to collect in situ surface wind observations over the southern New England continental shelf in order to calibrate and validate the ability of land-based HF radars to observe spatially variable surface winds over the coastal ocean. Specifically, this project aimed to produce radar-based estimates of wind speed and direction, with documented errors, over the domain of an HF radar system using mobile autonomous surface vehicles (ASV). The study area south of Martha's Vineyard, Massachusetts (Fig. 1), is observed by the high-resolution radar systems

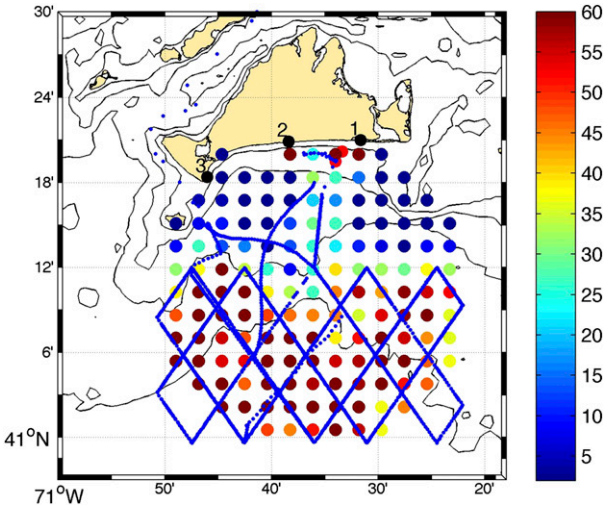

FIG. 1. Plan view of the amount and locations of independent wind samples (colored circles) collected at grid points of the WHOI radar system, shown at the spatial resolution of the WHOI system. Radar site locations 1–3 (black) are numbered from east to west. The ASV track line is shown in blue. Bathymetry is shown in 10-m increments.

operated by the Woods Hole Oceanographic Institution (WHOI) (Kirincich et al. 2012, 2013) and is an area of interest for wind power development. This work was timed to leverage a temporary expansion of the system's footprint that would maximize overlap with the Massachusetts Wind Energy Area. The manuscript is organized as follows: More information on radar sensing of the sea surface is given next, followed by the datasets, their processing, and details of the model formulation used here and its justification. The calibration and validation of the model and the empirical coefficients specific to the WHOI radar system are then presented, followed by an analysis of the results and a discussion of the successes, failures, and potential future relevance of the technique.

2. Background

This study seeks to develop and test empirical transfer functions to predict the real-time spatial structure of near-surface winds over the coastal ocean using HF radar backscatter power. This work focuses on the information contained in the strongest portion of the radar return from the sea surface, the first-order region (Barrick 1972). Returns within this first-order region are solely the result of "Bragg scattering" off surface gravity waves with a wavelength one-half the radar transmit wavelength as opposed to weaker power returns that flank the first-order region—that is, the "second order" region—due to double scattering or nonlinearities in the wave field. For the transmission frequencies used by the

WHOI system, 25 MHz, this corresponds to a ''Bragg wave'' with a wavelength of 6 m and a period of 2 s. In typical coastal environments, the Bragg waves associated with HF radar systems are directly forced by the local winds. For the WHOI systems in particular, the Bragg waves and their energy follow the wind speed and direction closely for wind speeds of 2–9 m s^{-1} for most fetch and/or wave age conditions (see Shen et al. 2012). Thus, this work assumes a direct relationship between the speed and direction of the wind and the direction and energy level of the Bragg waves observed by the radar.

Relating the wind vector field to the power of the first-order backscatter spectra due to Bragg waves is preferable to, for example, relating either winds to the measured currents or the full directional wave spectrum itself. The relationship between winds and surface currents is complex due to the effects of rotation and stratification, as well as the myriad of other forcings that can drive currents in the coastal ocean. Additionally, currents respond much more slowly to the wind than short waves. Second, HF radar–based extractions of the winds are possible via inversions of the second-order backscatter power (Barrick and Weber 1977; Lipa 1978; Lipa and Barrick 1986; Wyatt 2000; Wyatt et al. 2003; Hisaki 2004; Green and Wyatt 2006) to first estimate the full directional wave spectrum. The energy levels of waves forced directly by the local winds are likely to be wind speed dependent in typical coastal environments, and these waves include, and can be longer than, the Bragg waves. Hence, if the high-frequency part of the ocean long-wave spectrum can be recovered from an inverse, then the wind speed and direction can be estimated directly via wind-wave spreading models. However, full inversions such as this are more limited in range due to signal-to-noise issues and can only be used by a small subset of the operational HF radar systems. More importantly, spectral noise is a critical issue in this calculation, and it has generally thwarted efforts to perform more complex extractions at time scales less than a few hours (Wyatt 2000; Wyatt et al. 2011). Finally, the potential role of bimodal wave distributions in influencing a full inversion for waves was addressed by Heron (2004), suggesting that even if the directional spectrum can be resolved, extracting the wind field from the spectral rolloff can be challenging.

The products possible from the first-order region and the low-order inverses are focused on exclusively here, as the longer time scales and reduced ranges over which full spectral extractions using the second-order portion of the spectrum or transformations from currents are not operationally useful. Thus, this work attempts to empirically determine the relationship between radar power in the first-order region and wind speed and direction. Encompassing scattering purely from the Bragg waves, the link between first-order energy and wind input energy is more simplistic (Shen et al. 2012). However, extrapolating the power of the Bragg waves to estimate the surface wind relies on the use of a model of wind-wave directional spreading as a basis function. A number of works (e.g., Heron and Rose 1986; Paduan et al. 1999; Shen et al. 2012; Wyatt 2012) have reviewed the development of models that explain the directional spreading of wind-driven waves away from peak power downwind. While the shape of the distribution can vary among the methods, generally all have assumed that the ratio of the energy in the Bragg waves traveling directly toward and directly away from the radar is a function only of the angle between the direction to the radar and the direction to the wind. Field results matching the spreading patterns and amplitudes observed by the radars themselves to models have somewhat mixed results (Wyatt 2012; Kirincich 2013), suggesting that additional model validation for the spreading model itself appears necessary.

3. Data and methods

During the 6-month period spanning from June to December 2014, three 25-MHz Codar Seasonde–type HF radar systems owned by WHOI were operated in an expanded domain from that described in Kirincich et al. (2012), collecting surface current observations up to 40 km offshore at resolutions ranging from 400 m onshore to 800 m at ranges of 15–40 km offshore (Fig. 1). Data from the WHOI radar system were processed following the advanced methods described in Kirincich et al. (2012). Specific to the present study, the raw HF radar backscatter returns were processed to yield the range and bearing of each significant return located within the Bragg (or first order) region using the multiple signal classification (MUSIC) direction-finding algorithm (Schmidt 1986) and a standard set of MUSIC parameters for Seasonde systems (Lipa et al. 2006). Time series of MUSIC-estimated signal power (see Kirincich et al. 2012 for details) for both incoming and outgoing waves at each location on a 2 km × 2 km grid were found by averaging all results within a 2-km radius for nonoverlapping 15-min periods. The resulting spatial coverage and mean power distributions from each of the three radar sites are shown in Fig. 2.

To document the relationship between radar backscatter power and surface winds within the northern extent of the Massachusetts Wind Energy Area, generally located offshore of the 30-m isobath (Fig. 1), the project deployed a Liquid Robotics Wave Glider ASV

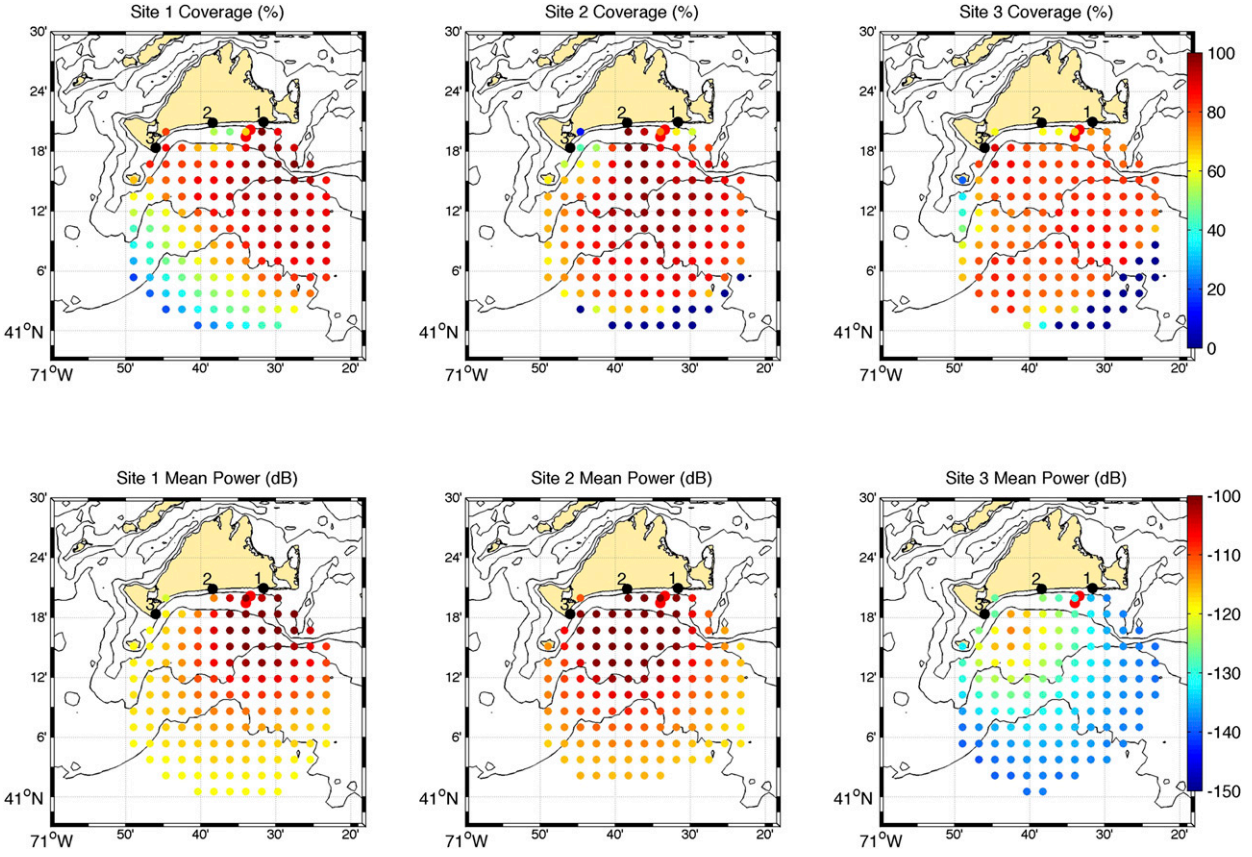

FIG. 2. (top) Percent coverage and (bottom) mean power for radar sites 1–3 from left to right. Coverage is defined as the number of 15-min averages from the site existing at a location for the month of November 2014. Mean backscatter power is in decibels.

during a 35-day period spanning 30 October–4 December 2014. The ASV was outfitted with an Airmar two-axis sonic anemometer measuring 10-min averages of wind speed and direction 1 m above the level of the vehicle. The ASV followed a predetermined path consisting of a series of 14 waypoints designed to cover the outer half of the existing radar coverage area with as many independent estimates of the wind speed and direction as possible. At average speeds of 1 kt (0.51 m s^{-1}), the full pattern was occupied in less than 9 days and was repeated almost 4 times during the project period (Fig. 1). The ASV updated its position, vehicle health information, and recent science observations every 10–20 min via Iridium communications.

Despite the rough weather conditions present during the deployment period, ASV operation was mostly autonomous, requiring the attention of an operator for, on average, less than 20 min day^{-1}. Deployment and recovery was made via the R/V *Tioga*, WHOI's 60-ft coastal research vessel, although a mid-deployment repair of the meteorological sensor was made using a smaller 25-ft vessel. Thus, despite some complications, the ASV deployment was successful, in that it 1) collected between 15 and 30 statistically independent samples of the near-surface wind conditions in each of the 106 project-defined grid cells spanning a combined 870-km^2 area (Fig. 1) over the course of a relatively short deployment period and 2) and utilized minimal resources beyond the acquisition of the vehicle itself.

Data from the ASV-based mobile wind sensor was augmented by wind observations collected by fixed meteorological stations at two of the land-based radar sites and the Martha's Vineyard Coastal Observatory's (MVCO) offshore tower (Fig. 1), all located inshore of the ASV-occupied area. All wind data were processed using standard quality assurance–quality control (QAQC) techniques to eliminate low-quality data and convert observations, made at heights ranging from 1 to 18 m to standardized 10-m reference height winds assuming neutral stability (Large and Pond 1981). For the ASV winds, much of the "low quality" wind data from the ASV resulted from either 1) times when the wind sensor was failing (one had to be replaced mid-deployment) or 2) times when there was a sampling issue

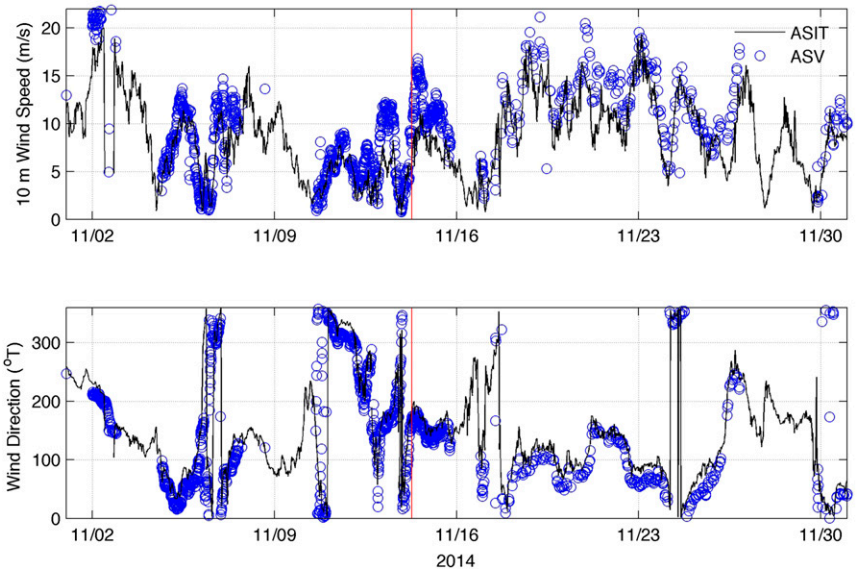

FIG. 3. (top) Wind direction and (bottom) speed as measured at the MVCO offshore tower and the ASV. The red line marks the winds during the period shown in Fig. 10.

between the AirMar and the ASV which led to shorter (1–5 min) averages of the wind results being transmitted as the 10-min averaged winds. In total <5% of the ASV data was eliminated by this QAQC step.

Wind observations were averaged onto a 15-min time series to match the common period of the radars. Winds collected on the offshore tower [Air–Sea Interaction Tower (ASIT)] were considered to be the least biased by potential orographic effects onshore, or wave sheltering offshore. While a suite of different sensors, including Vaisala three-axis and two-axis sonic anemometers and the Airmar compact two-axis sensor, were used to provide wind data, the differences between the sensor quality and measurement heights were small relative to the potential differences due to the spatial structure of the wind field and/or orographic effects for the onshore sensors. As shown in Fig. 3, the adjusted mobile wind results are similar to the ASIT winds at lower frequencies of variability but differ in both the absolute speed and timing of transitions.

During the study period, marking the transition to winter conditions over the New England shelf, winds were highly variable in both speed and direction. While the time-averaged wind speed was $7.5\,\mathrm{m\,s^{-1}}$ with a standard deviation of $4\,\mathrm{m\,s^{-1}}$, several storms occurred during the month with wind speeds greater than $10\,\mathrm{m\,s^{-1}}$. This study focuses on winds less than $10\,\mathrm{m\,s^{-1}}$ for two reasons: 1) $10\,\mathrm{m\,s^{-1}}$ is above the equilibrium range for the Bragg waves examined here (Shen et al. 2012) and 2) offshore wind energy production in the region is likely to have the greatest impact during the spring and summer periods, when demand for electricity is highest and winds are typically weaker than $7\,\mathrm{m\,s^{-1}}$ with mean wind speeds of $4 \pm 2\,\mathrm{m\,s^{-1}}$ (Fewings et al. 2008). Despite this restriction, distributing the ASV-based wind observations onto the same 2-km grid used for the radar observations resulted in more than 15 independent samples (defined here as wind observations greater than 3 h apart) of the wind spread out over the deployment month at all locations within the ASV deployment area. A number of the grid locations had more than 25 samples, and a majority had samples from three or more directional quadrants.

4. Model formulation

a. *Comparison of observed Bragg ratio to existing models*

A number of models for the directional spreading of wind-generated waves have been proposed and utilized with HF radar observations to extract information about the surface wind direction (see Wyatt 2012 for a review). As described above, the directional spreading of wind waves and thus information about the wind direction itself is seen in the signal received from HF radars via the difference between the backscattered power from waves coming directly toward and those moving directly away from the radar. The ratio, or difference of these powers, can be exploited to remotely sense the wind direction, assuming that the Bragg waves are in equilibrium with the local winds. A plot of this ratio by wind direction as observed by radar site 3 offshore (Fig. 4)

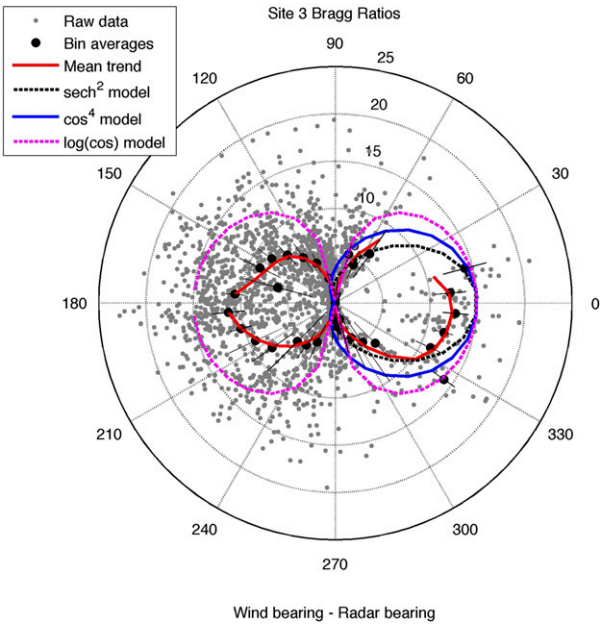

FIG. 4. Bragg ratios at a central site (41°10′N, 70°35′W) as sensed from site 3 and organized by the relative angle of the wind to the bearing between the radar and the site. Bin averages, by azimuth, of the Bragg ratios (red curve and black circles with standard error) are also shown along with common estimates of the functional form of the Bragg ratios directional dependence, scaled to match the observations.

illustrates two main points: 1) The mean relationship between the radar backscatter ratio, shown by the circles (bin averages) and red line (moving average), is fairly smooth and in general representative of a hyperbolic secant (as sech^2 or equivalent) type of shape; and 2) there is significant variability or noise of the individual results about the smoothed pattern shown that suggests, regardless of the functional form, any viable model solution would have to account for this variability to be successful.

Additionally, time series of the difference between the observed Bragg ratio and a time series of the mean Bragg ratio for the observed radar–wind direction, defined here as the ''residual'' Bragg ratio, from all three sites were positively correlated at any given location. This correlation suggests that the drivers of the residual or noise about the mean Bragg ratio must have either large spatial scales relative to the array itself or be the result of locally driven oceanic process that affects the returns of all radars. The correspondence of the mean Bragg ratio to the models shown in Fig. 4 breaks down for azimuthal directions observing winds with potentially limited fetch. This effect is more clearly seen in the results captured by sites 2 and 1, which more often have ''offshore'' winds. Thus, analysis of these results suggests that the variability seen is coherent across the radars for a given time and location, potentially due to variability in wave age, the wave environment, or the wind speed itself. This variability does not appear to be due to incoherent internal radar noise as deviations from the mean functional form are correlated across all the radars. If true, a directional model fit to the data that incorporates a parameter or parameters to represent this variability should be able to achieve more successful results than an application of a standard spreading model with a constant offset for the internal radar power.

b. Empirical link between power and speed

An examination of the relationship between observed radar power within the Bragg peaks and wind speed for times when the winds were directly toward or away from the radar—with no directional dependence present—illustrates that radar power has a clear dependence on wind speed. Utilizing the longer wind record available at ASIT, the radar power from the range–azimuthal cells overlapping the ASIT location from each radar illustrates that, whether at close or moderate ranges from the radar (i.e., Fig. 1), an increase in power of 5–20 dB with increasing wind speed occurs for all sites (Fig. 5). Additionally, separating the collocated wind and radar results for moderate and longer ranges for times when the ASV-measured wind was directly toward or directly away from the radar illustrates both the wind speed dependence of power and the range dependence of the wind speed effect (Fig. 5).

Despite the fact that these relationships appear both spatially variable and nonlinear, much of the patterns seen can be explained by a small number of key factors. First, there is an overall decrease in power with range due to a range-dependent attenuation. Second, for low winds the magnitude of the increase in power for increasing wind speed tends to decrease with range. Third, at higher wind speeds, generally greater than 5 m s^{-1}, the observed power increase either tapers off or actually decreases with increasing wind speed. This falloff can be attributed to increased winds, causing increased waves of all wavelengths, which increase scattering and power loss of the radar signal. Finally, the results have the potential to be noisy. Despite the advanced quality control practices used on the radar dataset, significant scatter exists that may complicate estimates of wind speed. However, focusing on the results at ASIT (Fig. 5, top), the scatter is notably different depending on wave/wind direction. As ASIT is west of site 1 and east of sites 2 and 3, waves/winds to the ''east'' have positive wind speeds at site 1 and negative wind speeds at sites 2 and 3, all of which have larger scatter than waves of the

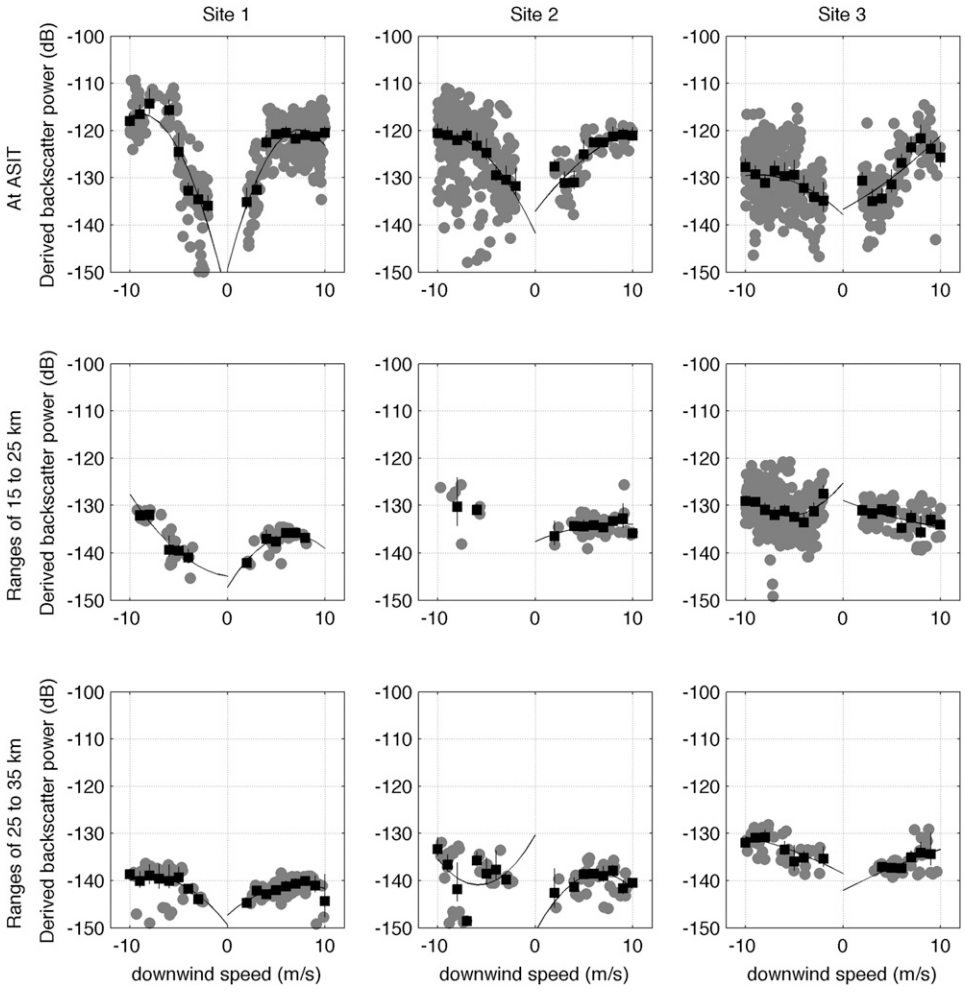

FIG. 5. Downwind speed (m s^{-1}) verses observed backscatter power for each of the WHOI radars (from left to right) at (top) ASIT (i.e., variable range), and ranges of (middle) 15–25 km and (bottom) 25–35 km. In all panels, the raw estimates (gray), bin averages (black), and quadratic regressions (black lines) are shown.

opposite direction, particularly for sites 2 and 3. Here, the limited fetch conditions present might account for the scatter seen.

Thus, the relationship between power and speed consists of variations around a spatially dependent mean value driven by a combination of increasing power due to higher winds and decreasing power due to increased attenuation. This type of potentially simple relationship exists between the mean power and wind speeds for all sites.

c. *Description of best-fit model*

The model chosen here to approximate the azimuthal variation in wave energy around the wind direction, as represented by Shen et al. (2012) and Gurgel et al. (2006), is

$$G(\theta) = 0.5\beta \operatorname{sech}^2(\beta\theta), \tag{1}$$

where G is the direction dependence (θ) of the wave energy and

$$\beta = \begin{cases} 2.28(f/f_p)^{-0.65}, & 0.97 < f/f_p \le 2.56, \\ 10^{-0.4+0.8393\exp[-0.567\ln(f/f_p)]}, & f/f_p > 2.56. \end{cases} \tag{2}$$

For HF radar data, f is the frequency of the Bragg waves of interest and f_p, where

$$f_p = \frac{11}{\pi}\left(\frac{g^2}{U_{10}F}\right)^{1/3} \tag{3}$$

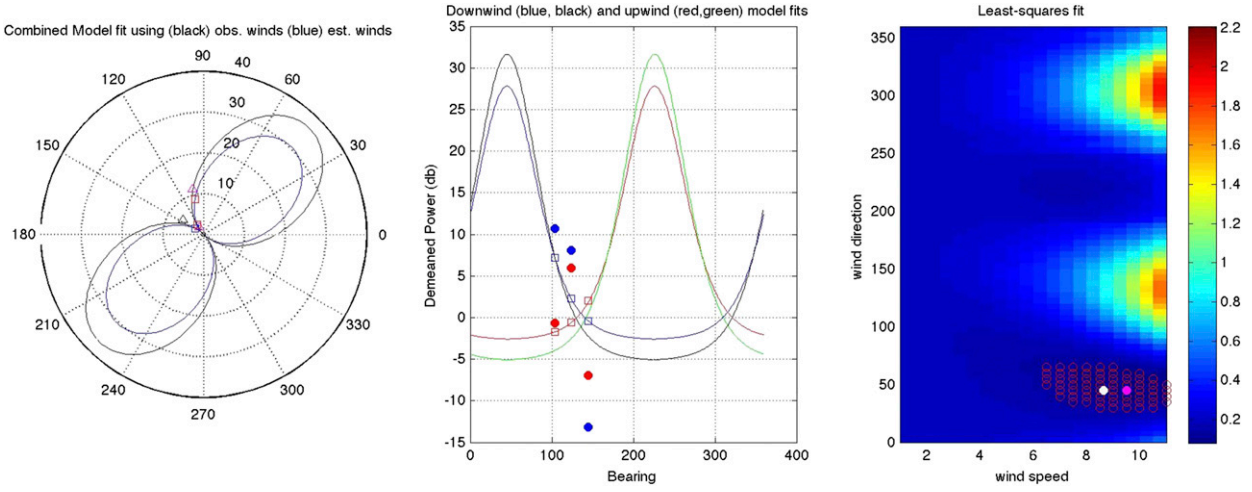

FIG. 6. Sample of the model fit methodology for a wind to the northeast, or toward 45° as shown in mathematical convention. (left) The absolute values of the Bragg ratios observed by the WHOI radars (triangles) and the best-fit model (black) along with the reverse-fit model made using the true wind and the estimated coefficients (blue line) and the inferred Bragg ratios from this model fit (open squares). (middle) The downwind (blue, black) and upwind (red, green) components of the best-fit model (blue, red) and the reverse-fit model (black, green) are shown with the observed (closed circles) and estimated (open squares) relative (as absolute mean) powers for the incoming (blue) and outgoing (red) Bragg waves. See text for details. (right) The least squares fit cost function with the extracted (closed magenta circle, found by the minimum value of the cost function) and observed (white circle) wind speed and direction and the confidence interval of the wind extraction (open magenta circles).

is the frequency of the dominant wave in equilibrium with the wind. Finally, g, U_{10}, and F represent gravity, the wind speed, and the fetch, respectively. A key aspect of using a sech^2 basis function, first presented by Donelan and Pierson (1987), as opposed to others that have been proposed (see Paduan et al. 1999 for a summary) is that the basis function is continuous over the full range of azimuthal directions in the format utilized in Fig. 6. Thus, the model can be used to estimate the wind direction (θ), from the distribution of the backscatter differences measured by two or more instruments. While the model for spreading has a wind speed dependence in β, the results of Fig. 5 show that the appropriate scaling factor to relate the value of G to the Bragg ratio must also have a wind speed dependence, and be much larger than 0.5β as shown above. Rescaling $G(\theta)$, the model appears to match the shape of the directional distributions shown here (Fig. 4) reasonably well.

Despite the complex physics governing the transfer of wind energy to ocean waves and the remote sensing of those waves by HF radar, the relationships shown in Fig. 5 can be approximated as an increase in power above a mean state due to increased wave energy competing with a potential decrease in power from increases in range or attenuation due to the additional roughness present at higher winds. Thus, power (P) at the Bragg frequencies (f) can be represented as

$$P(\pm f) = \kappa + E, \tag{4}$$

where κ is a location-dependent reference power and E is the difference in power above this reference that is due to the increased energy of the Bragg waves as a result of wind forcing. While κ could be modeled based on a radar's transmit power, beam spreading, and attenuation, in practice simply using the time series mean power observed at each location (i.e., Fig. 2) from each radar results in a better starting point as it accounts for real variations in the spreading and loss of the radar signal. Then, E might go as $E = Ew + Ea$, where

$$Ew = W_{\text{fact}}(U_{10}/c)^2 \tag{5}$$

and

$$Ea = -(r/r_{\max})(U_{10}/R_{\text{fact}})^3. \tag{6}$$

As formulated, Ew represents the form of a typical wave energy growth equation, with U_{10} being the wind speed and c being the phase speed of the Bragg wave, times W_{fact}, a constant that represents the power gained per unit wind at each location. The term Ea is empirically determined to best represent the decrease in power with increasing range, assumed to be linear, and the increase in attenuation with wind speed (U_{10}/R_{fact}), where R_{fact} is a constant that determines the importance of the power loss term. In practice, the exponent of U_{10}/R_{fact}, assumed to be cubic here, must be greater than the exponent of U_{10}/c, to obtain the

observed rolloff of power with increasing wind speed. With this formulation, the combination of W_{fact} and R_{fact} can be tuned to mirror any of the profiles seen in Fig. 5. Thus, the combined model used to represent the total power is

$$P(\pm f) = \kappa + (Ew + Ea)\,\text{sech}^2(\beta\theta). \quad (7)$$

5. Model calibration and validation

As written, the model can be used to convert wind speed and direction directly to signal power at a radar, given a known set of constants (W_{fact} and R_{fact}). Alternatively, as a linear set of equations for any number of radar stations (a minimum of two is needed), the model can be solved in the least squares sense for the wind speed and direction given observed signal powers and known model coefficients. The model coefficients themselves can be estimated for each spatial location by calculating the modeled signal powers for the entire parameter range of coefficients given the observed winds and minimizing a cost function defined by the normalized sum of three parameters: the average difference between the modeled and observed Bragg ratios; the incoming Bragg wave power anomaly, or $P(+f) - \sum[P(+f)]$; and the outgoing Bragg wave power anomaly, or $P(-f) - \sum[P(-f)]$. This combination of parameters was found to give a cost function with potentially high gradients as a function of both W_{fact} and R_{fact}. The methodology was tested extensively with synthetic data as follows:

1) Estimate the signal powers for an arbitrary set of wind and coefficient data.
2) Add noise to the estimated signal powers and then use with the known winds to estimate the model coefficients via use of the cost function.
3) Use the mean value of the coefficients from (2) with the noisy signal powers to estimate the wind speed and direction via use of the cost function.

As formulated, with up to 50% random error assigned to the synthetic signal powers (noise with a maximum of 50% of the power anomaly, but a mean of 30%), the process was able predict the wind direction and speed with RMS differences of 37° and 0.75 m s^{-1}, respectively. For real data, only step 2 (the calibration step) and step 3 (the wind estimate step) are used. The cost function used in step 3 also provides an uncertainty estimate for the wind speed/direction calculation, defined as the range over which the cost function value is less than 5% of its full range above the minimum value (Fig. 6). The value of 5% was chosen based on the consistency of the results described below. The solution space for the cost function potentially had other local minima, but tests showed that the global minima were most often related to the correct solution.

6. Analysis of results

a. *Empirically determined coefficients and their variability*

To determine the calibration coefficients, a subset (generally half) of the paired wind and radar data having returns for both $P(+f)$ and $P(-f)$ from all three radar sites, and wind speeds between 2 and 10 m s^{-1} were used. Again, the observed radar backscatter power was first used in a backward step to isolate the coefficient values that best fit the data using the known winds via the model. The results of this first step (step 2 above) for all areas within the domain that have greater than 10 calibration samples obtained from two or more separate wind quadrants have a few clear trends (Fig. 7). As shown, the combination of using the difference from the local mean power and the range factor (r/r_{max}) accounted for much of the range-dependent decrease in the absolute value and gain of the wind speed dependence (Fig. 5) as there is no real offshore trend in the value of R_{fact}.

However, spatial structure still exists in both coefficients, and it can be characterized by slowly varying spatial trends throughout much of the domain except for near the edges, where calibration data were more limited (Fig. 7). Except for key outliers, most of the mean W_{fact} values range between 0.5 and 2. Both outliers and areas along the northern edge of the domain with high standard deviations may be related more to poor sampling of the wind or the limited number of samples (i.e., Fig. 1) than to a marked change in the true value of the coefficients themselves. High values of mean R_{fact} offshore and to the west appear to coincide more with the area of decreased mean power from site 1 (Fig. 2) as opposed to simply increased offshore distances. A weaker azimuthal trend with higher values in the middle exists in W_{fact}, but it is dwarfed by higher values to the north and south. In general, these results tend to support the assumption that azimuthal variability in the response of the radar antenna system plays an important role in setting the coefficient values (see Shen et al. 2012).

A number of the locations had significant scatter about the mean values. In an attempt to include this variability in the model fits, coefficient values that were dependent on the wind speed, for example, were investigated via regressions to the observed scatter of the

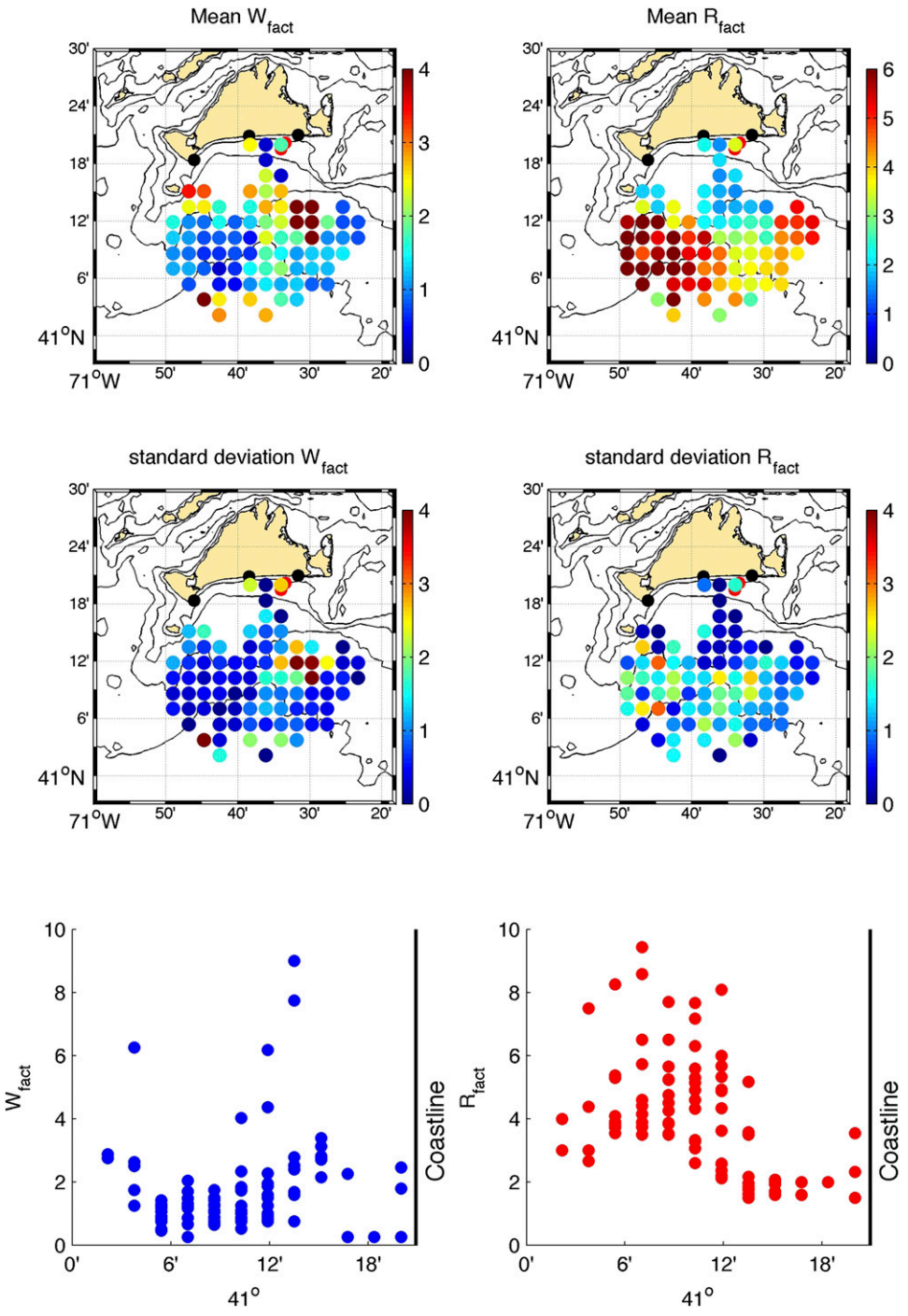

FIG. 7. Estimated (top) mean and (middle) standard deviations for (right) W_{fact} and (left) R_{fact} at each grid location of the radar fields, and (bottom) the latitudinal variability in both coefficients.

coefficients for a given location. However, as much of the variability appeared more as noise around the mean than a significant trend in wind speed, or any other known parameter, use of variable coefficients did not result in better extractions of the wind. Testing the significance of the results further, the spatially dependent mean values of the coefficients performed better than a single spatially uniform set of coefficients and better than the unit value for the coefficients. Finally, using the longer time series available at the

onshore wind stations, little variability in the derived mean coefficients was found over time. Thus, with the exceptions given above, the mean values of the coefficients appear to be the best indicator of the expected value of the result.

Further efforts to understand the drivers of the coefficient variability are of critical importance as areas with a higher standard deviation in the coefficient values tend to also have higher error rates, as shown below. Potential sources of variability include fetch or wave age issues, sampling issues, variable radar attenuation due to local radar-site variability and potential errors in the model solution, radar processing, or wind observations themselves. Additional effort is needed to test the effects of these processes on the scatter or uncertainty of the coefficients, and how this knowledge can be incorporated into improvements to the model.

b. *Error estimates*

Aggregating the results for all potential locations, the rms differences between the estimated and observed 15-min averages of wind speed and direction were calculated for three different comparisons:

1) Using only the calibration dataset, with the individual constants determined for each instance
2) Using only the calibration dataset, with the mean constants for each location
3) Using all viable two- or three-site datasets with the mean constants for each location

The model predictions have rms differences in wind direction between 35° and 40°, independent of how the coefficients are used or the wind speed itself. Results for the method's ability to predict wind speed, as the rms difference between observed and extracted winds, are shown in Fig. 8 for each of these three cases: all winds, and wind speed ranges of 2–6 and 6–10 $m\,s^{-1}$, respectively.

The first comparison gives an estimate of the internal noise of the calibration itself, or how well the radar and wind observations can match given the model formulation. As would be expected, this comparison has the lowest rms differences, with values of 1.2–1.7 $m\,s^{-1}$ for low to high wind speeds. The errors shown here represent a baseline error estimate of the correspondence between the measured winds and the observed power results themselves. For example, if the radar power observations were not consistent with the observed wind direction, the forward fit using the exact coefficients determined by the backward fit might not result in an extracted wind speed or direction similar to the observed winds.

Applied to both the second and third comparisons, either the calibration dataset only or all viable data with in situ validation using the spatially variable mean coefficients, the rms difference results have similar error statistics (Fig. 8). For both, rms differences increase to 1.4 and 2.7 $m\,s^{-1}$ for low and high winds, respectively. The similarity between the second and third comparisons suggests two conclusions: that the increase in errors due to the use of the mean rather than time-varying coefficients is the primary source of the increase in error above the first comparison, and that the calibration dataset was sufficient, relative to all data, with in situ validation to capture the mean coefficient, on average. An important caveat to this is those locations at the northern end of the area with poor in situ wind coverage. As the time-varying coefficients cannot be known for all times, the mean relationship must be used. Thus, the two major sources of error moving forward are 1) how well the model itself is able to fit the data and the wind and 2) how much temporal variability exists in the true coefficients. Both are discussed below.

Importantly, while the systemwide rms difference is 2.1 $m\,s^{-1}$ using the mean coefficients, comparisons at higher wind speeds are significantly worse than the overall mean. As Fig. 5 illustrates, the range of power variations at higher wind speeds is quite small, even for short ranges. Thus, it is not unexpected that the comparisons would degrade rapidly with increased speeds. These results suggest that 25-MHz radar systems may not be able to sufficiently observe wind speeds greater than 6–7 $m\,s^{-1}$ alone. Restricted to lower winds where the system, as deployed, is better suited gives error rates of 1.4 $m\,s^{-1}$ or less. However, that rms difference magnitudes for wind direction do not vary between the comparisons suggests that much of the directional error is due to misfits of the model itself and not due to wind speed or coefficient variability. These types of errors are discussed in more detail below.

These error rates are either at par with, for larger wind speeds, or slightly less than, for smaller wind speeds, similar error metrics for other remotely sensed wind products. For example, a number of recent studies have compared remote QuikSCAT or similar satellite-based extractions for wind speed and direction to in situ, normally buoy-based, wind observations (Carvalho et al. 2014) and various reanalysis products (see Carvalho et al. 2012), finding rms errors for speed and direction of 1.7–2 $m\,s^{-1}$ and 40°–50°, respectively. Synthetic aperture radar (SAR) satellite–based winds have been shown to have rms errors of 2 $m\,s^{-1}$ and directional ambiguities of ±40° (Fisher et al. 2008). While generally comparable to that shown here, it is important to note that only SAR observations have potential resolutions that approach

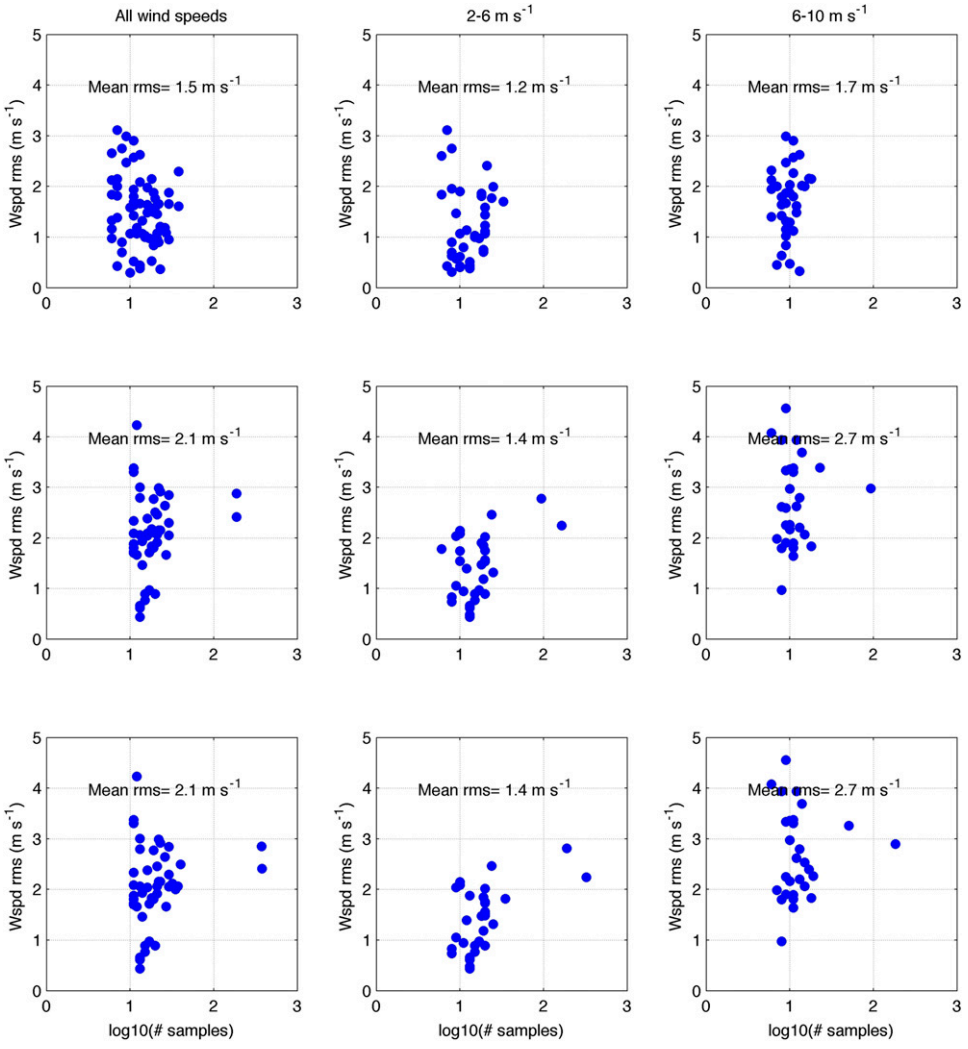

FIG. 8. RMS differences between measured and estimated wind speeds for all locations, shown for (left to right) all wind speeds, and 2–6 and 6–10 m s^{-1} using (top) the calibration dataset and individually estimated coefficients, (middle) the calibration dataset and mean coefficients, and (bottom) all available data with the mean calibrations.

HF radar in the coastal ocean and that none of these observational platforms has the temporal sampling abilities of HF radar.

c. *Demonstration of success, failures, and relevance of the technique*

An example of the potential HF radar wind extractions, compared to available validation data, is shown in Fig. 9. This comparison is illustrative of the potential areas of successful wind extractions and of areas needing improvement. For all the data shown from this location (located offshore and to the east), the rms differences in wind direction and speed were 45° and 2.2 m s^{-1}, respectively. The speed and direction are adequately predicted during samples 9–11 and 16–24, when the signal powers themselves have only a small range. However, areas of notable misfit also exist that are representative of the two types of errors encountered in the larger dataset.

The first type, found during samples 1–6, 12–15, and 25–28, is when the extracted wind speed grossly over- or underpredicts the observed winds. This type of error is of interest in that the signal powers span a wide range and the wind direction is potentially well resolved, but the model fit still poorly estimates the wind speed. It is suggested that the ambiguity of the wind speed model, particularly at the offshore locations, might be responsible for these types of errors. As shown in Fig. 5, the wind speed relationship is potentially parabolic in wind speed, and thus the solution could be multivalued for wind speeds of, for example, 4 or 8 m s^{-1}. However,

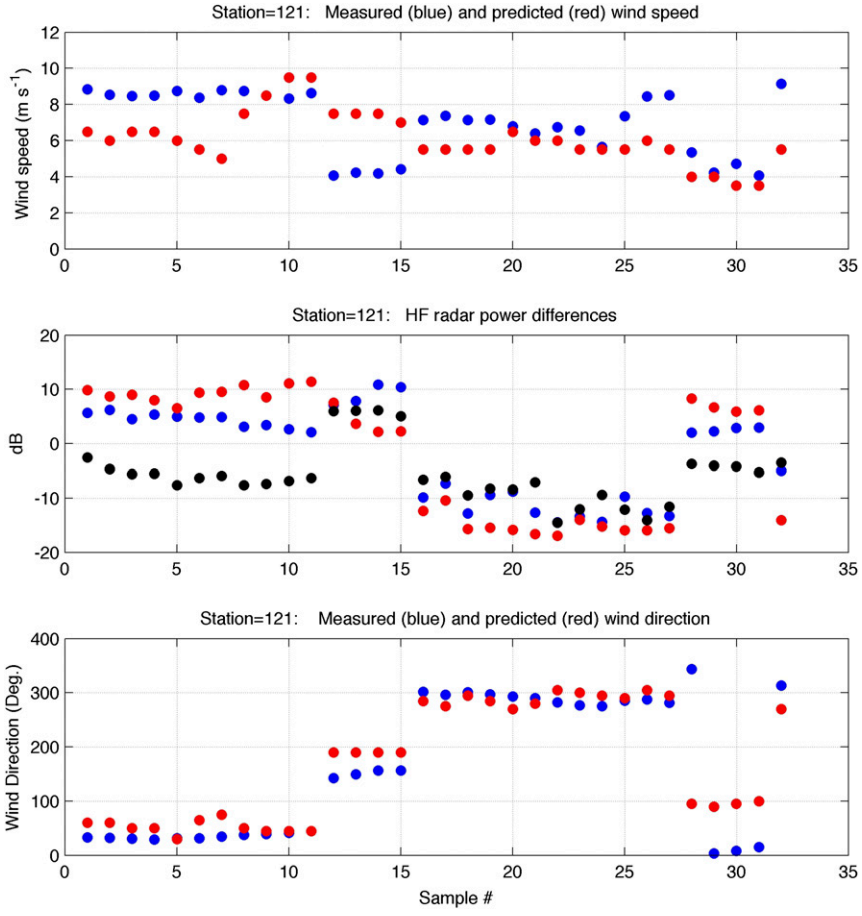

FIG. 9. Sample comparisons of the in situ measured and estimated (top) wind speed and (bottom) wind direction, and (middle) the observed radar power differences. Note the sample numbers do not represent a time series but are individual, independent estimates made throughout the analysis period.

other environmental factors—for example, rain—and their effects on the radar might also cause underpredictions by lowering the overall power for a given wind speed. It is not known how much rain specifically may have affected the dataset, but preliminary estimates suggest that it is not the primary driver of variability about the mean relationships. Finally, while it is unclear how much the lower power gains with increasing wind speed and range offshore may add to this issue, adding radar coverage from a different operating frequency would clearly mitigate many of these types of issues and greatly improve error estimates at higher winds. Further examination of the drivers of this type of error is an important topic for future efforts.

The second type of error, shown in samples 29–31 (Fig. 5), is when the wind speed is accurately predicted but the wind direction is poorly predicted. This indicates more a disagreement between the radar and the data than a potential failure of the model, and it may be the result of a breakdown of the assumption that the Bragg waves are following and responding to the wind (see Wyatt 2012) or errors in one or both of the observations. Analysis of the full dataset shows that these types of cases tend to have larger values of model-estimated error. However, the overall the difference between the observed and extracted winds is within the bounds of the model-estimated error 80% of the time. Thus, despite the fact that potentially large differences can exist between the extracted and observed winds, the wind extraction results are able to provide knowledge about when such errors are present.

Finally, it is useful to examine the potential role of the extracted wind results to provide details on the spatial structure of the wind field not possible via other, coarser sampling methods. Shown in Fig. 10 is the detailed structure of the extracted wind speed and direction at 0645 UTC 4 November 2014. As shown, the wind direction is predominately offshore to the south

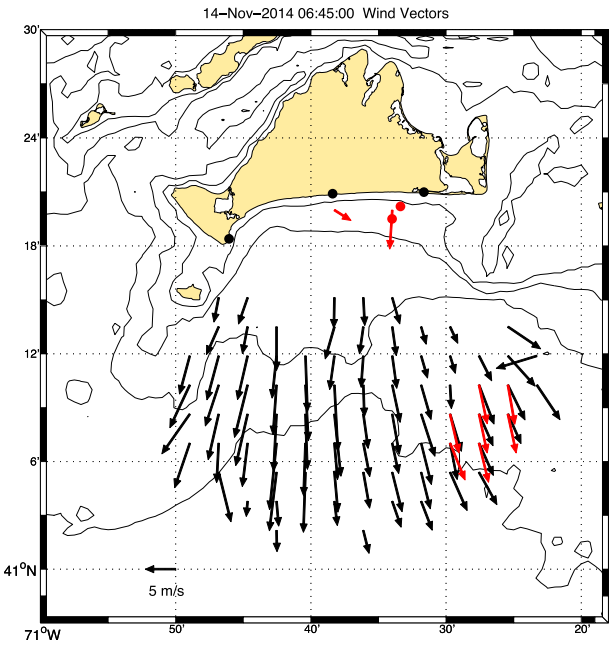

FIG. 10. Surface wind vectors at 0645 UTC 14 Nov 2014 sensed by the calibrated HF radar system (black) and in situ wind sensors (red). The mobile sensor was assumed representative of a 3-km watch circle.

throughout the domain with some apparent spreading away from directly south with longitude. The wind speed, however, varies more substantively, increasing from 4 to 10 m s^{-1} from east to west (Fig. 10). At the time of the sampling, the ASV was located on the eastern side of the area, and the mobile wind sensor agreed well with the local extractions. This example time period occurs at a time of rapidly increasing wind speed (Fig. 3), and the change in speed across the study area is consistent with a weather feature propagating through the region. Thus, while the intermittent over-/underprediction errors described above, which can be easily mitigated in future installations, add a note of caution in the interpretation of the present dataset, the radar results suggest that sizable spatial structure in the wind field may be present in the study area, and captured by the remote sensing methods described here.

7. Conclusions and recommendations

This work has demonstrated that remote observations of surface winds can be made via HF radar using low-cost deployments of autonomous surface vehicles to calibrate and validate empirical models linking wind speed and direction directly to the radar backscatter power. Using the method and calibration/validation techniques described above, HF radar remote extractions of surface winds have the following:

- RMS differences of 1.2–1.4 m s^{-1} within the observational range of interest here, nominally 2–6 m s^{-1} wind speeds
- RMS differences of 1.7–2.7 m s^{-1} for high wind speeds near the edge of the suitable ranges of the sensors and technique
- Uncertainties that are well characterized by the model-estimated uncertainty ranges, as 80% of differences between in situ and remote estimates were less than the uncertainty estimate given in the model.

It is important to note that the error values given here are for 15-min samples of the radar power and winds. Errors generally decrease with longer—30 min or hourly—averages, suggesting that short-term noise or model–data mismatches drive a portion of the errors seen.

The main goal of the study was to show the utility of a mobile wind sensor, combined with potentially simplified models and optimizations were able to reasonably observe the surface wind field remotely via HF radar. This work has shown that as few as 10–15 independent samples at each measurement location were sufficient, provided they spanned the distribution of the potential wind field present. Thus, potentially short deployments of an autonomous vehicle, or sparse shipboard observations of opportunity, could be used to calibrate an HF radar system for winds and to perform periodic validation.

However, the model developed and implemented here remains overly simplistic in a few key areas and there are numerous, more complex optimizations for the linear sets of equations examined here. Additional efforts in honing the model formulation are likely to provide the most substantial reductions in error. As stated in the text, 80% of the wind estimates where within the uncertainty metric of the wind extractions. Said differently, this shows that large differences between the data and radar estimates are more likely due to measurement error in the sensors or a poorly fitting model than the method used to optimize the solution. Thus, additional work should examine individual cases of high error rates to understand what factors in the data or model drove the misfit, as well as examine and understand the drivers for empirical constant variability. Are higher standard deviations in the empirical constants due to poor wind directional model fits, radar noise, or incorrect implementations of the wind speed dependence? Would a more careful accounting of other sources of power/intensity variability in the model formulation—that is, due to

ground wave propagation changes—lead to improved results?

Targeted changes or additions to the observational system used here would likely resolve many of the issues highlighted above. Many of the increased errors at higher wind speeds were due to low signal-to-noise ratios and the winds approaching or exceeding the theoretical limit of radar to wind correlation for the operating frequencies used. These issues could be further mitigated, or perhaps solved, by increased transmitting power (the WHOI systems were not operating at ''full'' power during the study period) and combining these observations with those of a second, lower-frequency system. This combination of multiple radar-operating frequencies—that is, the 25-MHz systems used here and an 11–13-MHz system—would enable data collection over a wider range, 2–14 $m\,s^{-1}$, of optimal wind speeds. Additionally, in situ estimates of surface winds by at least one buoy system in the area would allow real-time monitoring and adjustments of the extraction estimates, greatly enhancing confidence in the larger, potentially spatially variable results. Areas with multifrequency HF radar coverage and in situ buoy–based wind sampling exist in many coastal areas; thus, a focused effort to resolve these remaining issues could allow real-time surface wind monitoring via HF radar in many areas.

Finally, these results suggests that the technique could be useful for measuring near-surface winds over the coastal ocean remotely on an operational basis and would fill an important niche in our operational observations of coastal ocean winds. Existing observational systems, such as buoy-based point measurements and satellite-based scatterometery, provide either high temporal coverage or high spatial coverage, but not both. However, greater temporal and spatial resolution of the near-surface winds that drive ocean currents and impact coastal areas is necessary for a broad range of research, industry, and operational uses. Such a real-time, quality-controlled data product could support data-driven, high-resolution, short-term forecasting of coastal wind fields with well-characterized uncertainties, and enable an examination of atmospheric forcing of the ocean and its potential variability on a wider range of temporal and spatial scales.

Acknowledgments. This analysis was supported by the Massachusetts Clean Energy Center. The HF radar data used were obtained during projects supported by the National Science Foundation, the NOAA Integrated Ocean Observing System (IOOS), and internal funds from the Woods Hole Oceanographic Institution. The ASV wind and HF radar data used in this analysis are available upon request (akirincich@whoi.edu).

REFERENCES

Barrick, D. E., 1972: First-order theory and analysis of MF/HF/VHF scatter from the sea. *IEEE Trans. Antennas Propag.*, **20**, 2–10, doi:10.1109/TAP.1972.1140123.

——, and B. L. Weber, 1977: On the nonlinear theory for gravity waves on the ocean's surface. Part II: Interpretation and application. *J. Phys. Oceanogr.*, **7**, 11–21, doi:10.1175/1520-0485(1977)007<0011:OTNTFG>2.0.CO;2.

Beaucage, P., M. C. Brower, and J. Tensen, 2012: Evaluation of four numerical wind flow models for wind resource mapping. *Wind Energy*, **17**, 197–208, doi:10.1002/we.1568.

Carvalho, D., A. Rocha, and M. Gómez-Gesteira, 2012: Ocean surface wind simulation forced by different reanalyses: Comparison with observed data along the Iberian Peninsula coast. *Ocean Modell.*, **56**, 31–42, doi:10.1016/j.ocemod.2012.08.002.

——, ——, ——, and C. Silva Santos, 2014: Comparison of reanalyzed, analyzed, satellite-retrieved and NWP modelled winds with buoy data along the Iberian Peninsula coast. *Remote Sens. Environ.*, **152**, 480–492, doi:10.1016/j.rse.2014.07.017.

Donelan, A., and W. J. Pierson, 1987: Radar scattering and equilibrium ranges in wind-generated waves with application to scatterometry. *J. Geophys. Res.*, **92**, 4971–5029, doi:10.1029/JC092iC05p04971.

Edson, J., and Coauthors, 2007: The Coupled Boundary Layers and Air–Sea Transfer experiment in low winds. *Bull. Amer. Meteor. Soc.*, **88**, 341–356, doi:10.1175/BAMS-88-3-341.

Fewings, M., S. J. Lentz, and J. Fredericks, 2008: Observations of cross-shelf flow driven by cross-shelf winds on the inner continental shelf. *J. Phys. Oceanogr.*, **38**, 2358–2378, doi:10.1175/2008JPO3990.1.

Fisher, C. M., G. S. Young, N. S. Winstead, and J. D. Haqq-Misra, 2008: Comparison of synthetic aperture radar–derived wind speeds with buoy wind speeds along the mountainous Alaskan coast. *J. Appl. Meteor. Climatol.*, **47**, 1365–1376, doi:10.1175/2007JAMC1716.1.

Green, J., and L. R. Wyatt, 2006: Row-action inversion of the Barrick–Weber equations. *J. Atmos. Oceanic Technol.*, **23**, 501–510, doi:10.1175/JTECH1854.1.

Gurgel, K.-W., H.-H. Essen, and T. Schlick, 2006: An empirical method to derive ocean waves from second-order Bragg scattering: Prospects and limitations. *IEEE J. Oceanic Eng.*, **31**, 804–811, doi:10.1109/JOE.2006.886225.

Harlan, J. A., and T. M. Georges, 1994: An empirical relation between ocean-surface wind direction and the Bragg line ratio of HF radar sea echo spectra. *J. Geophys. Res.*, **99**, 7971–7978, doi:10.1029/93JC03560.

Heron, M., 2004: The effect of bimodal sea spectra on HF radar wind analysis. *Oceans '04: MTS/IEEE Techno-Ocean '04; Conference Proceedings*, Vol. 1, IEEE, 537–541, doi:10.1109/OCEANS.2004.1402972.

——, and R. Rose, 1986: On the application of HF ocean radar to the observation of temporal and spatial changes in wind direction. *IEEE J. Oceanic Eng.*, **11**, 210–218, doi:10.1109/JOE.1986.1145173.

Hisaki, Y., 2004: Short-wave directional distribution for first-order Bragg echoes of the HF ocean radars. *J. Atmos. Oceanic Technol.*, **21**, 105–121, doi:10.1175/1520-0426(2004)021<0105:SDDFFB>2.0.CO;2.

Kirincich, A. R., 2013: Toward real-time, remote observations of the coastal wind resource using high-frequency radar. *Mar. Technol. Soc. J.*, **47**, 206–217, doi:10.4031/MTSJ.47.4.22.

——, T. de Paolo, and E. Terrill, 2012: Improving HF radar estimates of surface currents using signal quality metrics, with application to the MVCO high-resolution radar system. *J. Atmos. Oceanic Technol.*, **29**, 1377–1390, doi:10.1175/JTECH-D-11-00160.1.

——, S. J. Lentz, J. T. Farrar, and N. K. Ganju, 2013: The spatial structure of tidal and mean circulation over the inner shelf south of Martha's Vineyard, Massachusetts. *J. Phys. Oceanogr.*, **43**, 1940–1958, doi:10.1175/JPO-D-13-020.1.

Large, W. G., and S. Pond, 1981: Open ocean momentum flux measurements in moderate to strong winds. *J. Phys. Oceanogr.*, **11**, 324–336, doi:10.1175/1520-0485(1981)011<0324:OOMFMI>2.0.CO;2.

Lipa, B. J., 1978: Inversion of second-order radar echoes from the sea. *J. Geophys. Res.*, **83**, 959–962, doi:10.1029/JC083iC02p00959.

——, and D. Barrick, 1986: Extraction of sea state from HF radar sea echo: Mathematical theory and modeling. *Radio Sci.*, **21**, 81–100, doi:10.1029/RS021i001p00081.

——, B. Nyden, D. S. Ullman, and E. Terrill, 2006: SeaSonde radial velocities: Derivation and internal consistency. *IEEE J. Oceanic Eng.*, **31**, 850–861, doi:10.1109/JOE.2006.886104.

Paduan, J. D., R. Delgado, J. F. Vesecky, Y. Fernandez, J. Daida, and C. Teague, 1999: Mapping coastal winds with HF radar. *Proceedings of the IEEE Sixth Working Conference on Current Measurement*, S. P. Anderson, Eds., IEEE, 28–32, doi:10.1109/CCM.1999.755209.

Schmidt, R. O., 1986: Multiple emitter location and signal parameter estimation. *IEEE Trans. Antenna Propag.*, **34**, 276–280, doi:10.1109/TAP.1986.1143830.

Shen, W., K.-W. Gurgel, G. Voulgaris, T. Schlick, and D. Stammer, 2012: Wind-speed inversion from HF radar first-order backscatter signal. *Ocean Dyn.*, **62**, 105–121, doi:10.1007/s10236-011-0465-9.

Wyatt, L. R., 2000: Limits to the inversion of HF radar backscatter for ocean wave measurement. *J. Atmos. Oceanic Technol.*, **17**, 1651–1665, doi:10.1175/1520-0426(2000)017<1651:LTTIOH>2.0.CO;2.

——, 2012: Shortwave direction and spreading measured with HF radar. *J. Atmos. Oceanic Technol.*, **29**, 286–299, doi:10.1175/JTECH-D-11-00096.1.

——, and Coauthors, 2003: Validation and intercomparisons of wave measurements and models during the EuroROSE experiments. *Coastal Eng.*, **48**, 1–28, doi:10.1016/S0378-3839(02)00157-6.

——, J. Green, and A. Middleditch, 2011: HF radar data quality requirements for wave measurement. *Coastal Eng.*, **58**, 327–336, doi:10.1016/j.coastaleng.2010.11.005.